




# Optimization of window settings for standard and advanced virtual monoenergetic imaging in abdominal dual-energy CT angiography

Damiano Caruso,<sup>1,2</sup> Ashley H. Parinella,<sup>1</sup> U. Joseph Schoepf ,<sup>1,3</sup> Maxwell H. Stroebel,<sup>1</sup> Stefanie Mangold,<sup>1,4</sup> Julian L. Wichmann,<sup>1,5</sup> Akos Varga-Szemes,<sup>1</sup> B. Devon Ball Jr,<sup>1</sup> Domenico De Santis,<sup>1,2</sup> Andrea Laghi,<sup>2</sup> Carlo N. De Cecco<sup>1</sup>

<sup>1</sup>Division of Cardiovascular Imaging, Department of Radiology and Radiological Science, Medical University of South Carolina, Ashley River Tower, MSC 226, 25 Courtenay Drive, Charleston, SC 29425, USA

<sup>2</sup>Department of Radiological Sciences, Oncological and Pathological Sciences, University of Rome “Sapienza”, Latina, Italy

<sup>3</sup>Division of Cardiology, Department of Medicine Medical, University of South Carolina, Charleston, SC, USA

<sup>4</sup>Department of Diagnostic and Interventional Radiology, Eberhard-Karls University Tuebingen, Tuebingen, Germany

<sup>5</sup>Department of Diagnostic and Interventional Radiology, University Hospital Frankfurt, Frankfurt, Germany

## Abstract

**Objectives:** To determine the optimal window setting for displaying virtual monoenergetic reconstructions of third generation dual-source, dual-energy CT (DECT) angiography of the abdomen.

**Methods:** Forty-five patients were evaluated with DECT angiography (90/150 kV, 180/90 ref. mAs). Three datasets were reconstructed: standard linear blending (M<sub>0.6</sub>), 70 keV traditional virtual monoenergetic (M70), and 40 keV advanced noise-optimized virtual monoenergetic (M40+). The best window setting (width and level, *W/L*) was assessed by two blinded observers and was correlated with aortic attenuation to obtain the Optimized *W/L* setting (O-*W/L*). Subjective image quality was assessed, and vessel diameters were measured to determine any possible influences between different *W/L* settings. Repeated measures of variance were used to evaluate comparison of *W/L* values, image quality, and vessel sizing between M<sub>0.6</sub>, M70, and M40+.

**Results:** The Best *W/L* (B-*W/L*) for M70 and M40+ was 880/280 and 1410/450, respectively. Results from regression analysis inferred an O-*W/L* of 850/270 for M70 and 1350/430 for M40+. Significant differences for *W* and *L* were found between the Best and the Optimized *W/L* for M40+, and between M70 and M40+ for both the Best and Optimized *W/L*. No significant differences for vessel measurements were found using the O-*W/L* for

M40+ compared to the standard M<sub>0.6</sub> ( $p \geq 0.16$ ), and significant differences were observed when using the B-*W/L* with M40+ compared to M<sub>0.6</sub> ( $p \leq 0.04$ ).

**Conclusion:** In order to optimize virtual monoenergetic imaging with both traditional M70 and advanced M40+, adjusting the *W/L* settings is necessary. Our results suggest a *W/L* setting of 850/270 for M70 and 1350/430 for M40+.

**Key words:** Dual-energy CT—Virtual monoenergetic—CT angiography—Window settings—*W/L*

## Abbreviations

M <sub>0.6</sub>	Standard linearly blended image
M70	Traditional virtual monoenergetic image at 70 keV
M40+	Advanced virtual monoenergetic image at 40 keV
B- <i>W/L</i>	Best <i>W/L</i> setting
O- <i>W/L</i>	Optimized <i>W/L</i> setting

Dual-energy computed tomography (DECT) operates by acquiring two datasets at different tube voltages and allows for material decomposition caused by attenuation differences at distinct energy levels [1, 2]. Moreover, DECT angiography is able to achieve diagnostic image quality despite using a reduced amount of contrast media

compared to the standard 120 kVp single-energy CT [3, 4]. This reduction provides higher detection rates for endoleak after aortic aneurysm repair [5], as well as the potential to reduce metal artifacts [6], ultimately improving endovascular stent visualization [7, 8].

DECT also enables the reconstruction of datasets at a desired, virtual monoenergetic spectrum (keV), allowing the highest contrast-to-noise ratio (CNR) to be obtained [9–11]. Previous studies have shown that DECT angiography virtual monoenergetic reconstruction at 70 keV has produced the highest CNR recordings to date [12]. Recently, a noise-optimized advanced image-based monoenergetic algorithm has been introduced to achieve superior CNR at lower keV levels (40 keV). This has been made possible by obtaining a balance between higher iodine attenuation and lower image noise [10, 13, 14].

DECT allows different intravascular attenuation values associated with different monoenergetic levels to be acquired. Virtual low keV levels increase intravascular attenuation [15], which requires adjustment of the display window settings [16]. Therefore, in order to attain similar image impressions compared to traditional settings, manual selection of image width ( $W$ ) and level ( $L$ ) is necessary.

To the best of our knowledge, no standardized window settings have been described regarding dual-energy CT angiography. Thus, the purpose of our study was to determine the most appropriate  $W/L$  settings and whether modification of the  $W/L$  settings is required for both the advanced virtual monoenergetic algorithm, as well as the traditional virtual monoenergetic algorithm compared to the standard 120 kVp.

## Materials and methods

### *Patient population*

This retrospective study was approved by our local institutional review board with a waiver of informed consent. From an initial cohort of 60 consecutive patients, we included 45 subjects (27 male and 18 female), who had undergone DECT angiography of the abdominal aorta and lower extremities for steno-occlusive disease ( $n = 21$ ), intermittent claudication ( $n = 18$ ), stent surveillance ( $n = 3$ ), traumatic injury ( $n = 2$ ), and aneurysm ( $n = 1$ ). Exclusion criteria for our retrospective study included any deviations from the DECT acquisition protocol ( $n = 12$ ) or contrast media injection protocol ( $n = 3$ ).

### *Dual-energy CT acquisition protocol*

All CT examinations were performed using a third generation, dual-source CT scanner (Somatom Definition Force; Siemens Healthcare, Forchheim, Germany). DECT images were acquired after intravenous contrast

media administration. Patients were examined in the supine position from the diaphragm to the tip of the toes to acquire the entire abdominal aorta and peripheral vessels. DECT arterial images were acquired using the following parameters: pitch 0.7, collimation  $2 \times 64 \times 0.6$  mm for both detectors, field of view 350 mm; tube A was operated at 90 kVp with a reference tube current of 180 mAs; tube B was operated at 150 kVp, equipped with an optimized integrated tin filter (Selective Photon Shield II, SPS II; Siemens) and a reference tube current of 90 mAs. Automated real-time anatomical tube current modulation (CareDose 4D, Siemens Healthcare) was activated for all acquisitions.

A fixed amount of 90 mL intravenous contrast material (Iohexol, Omnipaque 350, GE Healthcare, Milwaukee, WI) was administered using a peripheral vein at 4 mL/s. This injection was followed by a 50 mL saline flush using an automated dual-syringe power injector (Stellant D CT Injection System, Medrad, Inc., Warrendale, PA) through an 18-gauge IV access placed in a superficial vein in the antecubital fossa. Timing of the scan was determined using a dedicated bolus tracking software application (CareBolus, Siemens) with a region of interest (ROI) placed in the abdominal aorta, just below the diaphragmatic dome. A trigger threshold level of 100 HU with a 12-s delay was then selected for detection of bolus arrival (120 kV, 23 mAs).

### *Image reconstruction and post-processing*

Raw data were transferred onto a 3-dimensional workstation (Syngo.via, version VA30, Siemens Healthcare). Two reconstructions were performed using a quantitative DECT medium sharp kernel (Qr40). The first series was designed to approximate typical, clinical routine single-energy 120 kV images. This series was reconstructed using vendor-recommended standard settings to create a linearly blended image (M\_0.6), combining 60% of low tube voltage output and 40% of high tube voltage output. The second and the third image series were reconstructed as virtual monoenergetic images using a clinically available DECT application (CT Dual Energy; Siemens Healthcare). Although this algorithm allows for image reconstruction at energy levels ranging from 40 to 190 keV, a traditional virtual monoenergetic at 70 keV (M70) and an advanced virtual monoenergetic reconstruction at 40 keV (M40+) were both created. These selections were based on recommendations from prior studies [10, 13, 14].

### *Objective image evaluation*

Each image dataset was assessed by one radiologist (S.M.) with 5 years of cardiovascular imaging experience. Axial images were selected, and three regions of interest (ROIs) of 100 mm<sup>2</sup> were drawn in three con-

secutive sections of the abdominal aorta (at the level of celiac trunk), paraspinal muscle, and subcutaneous fat. Attenuation values, measured in Hounsfield Units (HU) and standard deviations (SD), were recorded, averaged, and compared for M<sub>0.6</sub>, M70, and M40+. Contrast-to-noise ratio (CNR) was calculated for each dataset using the following equation:  $(HU_{\text{aorta}} - HU_{\text{muscle}}) / SD_{\text{fat}}$ .

### Window settings

In the first part of the study, optimal window settings for M70 and M40+ were determined by two independent observers. Both observers evaluated each image dataset separately using a standard clinical PACS viewing system (IMPAX v.6.5, Agfa, Greenville, SC). The two observers had 5 (D.D.S.) and 7 (D.C.) years of cardiovascular imaging experience, respectively. *W/L* settings were manually adjusted by each observer to achieve the most suitable *W/L* combination with regard to the separation between vascular calcifications and intraluminal contrast. For every patient, the *W/L* settings for the arterial phase images were recorded in random order for both M70 and M40+. In addition, these settings were recorded in different interpretation sessions to avoid recall bias. Therefore, each observer documented two values for each dataset: one for *W* and one for *L*. The *W* and *L* values were then separately averaged between the two observers to establish the “Best *W/L*” (B-*W/L*) settings for M70 and M40+, which were applied in the next phase of the study.

The second phase of the study required a linear regression analysis between the B-*W/L* and the attenuation values of the aorta, as a major determinant of *W/L* selection [16]. Thus, for the M70 and M40+ datasets, the HU values of the aorta were plotted against window parameters (Best Width and Best Level) producing four scatterplots (two for each dataset). The derived scatterplots were used to elaborate separate linear regression lines resulting in first order equations. These equations were used to obtain the Optimized Width and Level and thus, to realize the “Optimized *W/L*” (O-*W/L*), which was expected to be highly correlated with intravascular attenuation.

### Subjective image evaluation

All datasets were evaluated by two additional observers with 12 (C.N.D.C.) and 10 (A.V.S.) years of cardiovascular imaging experience, respectively. Each observer was blinded to patient data and image reconstructions, and determined whether a qualitative difference existed between the datasets viewed at B-*W/L* and O-*W/L* for M70 and M40+ compared to the standard *W/L* of M<sub>0.6</sub>. Subjective image quality was rated based on sharpness and contour delineation, image noise, percep-

tion of calcifications from intra-aortic iodine contrast, and overall image quality, using a five-point Likert scale (1 = poor; 2 = fair; 3 = moderate; 4 = good; 5 = excellent) [17]. As a result, three datasets for each patient were analyzed, and then the scores were recorded and compared. To avoid recall bias, the two observers were blinded to the window settings. At the beginning of each interpretation session, a third observer (A.L.) manually obtained *W* and *L* for each exam and arranged the datasets in random order. A minimum of two weeks was required between each interpretation session, which involved anywhere from 5–10 exams.

Additionally, each observer manually measured the maximum diameter of the abdominal aorta (at the level of the celiac trunk origin), bilateral common iliac arteries, and bilateral common femoral arteries [18, 19]. Measurements were recorded, averaged, and compared to assess any possible influence of *W/L* settings on sizing.

### Statistical analysis

Continuous variables were expressed as mean  $\pm$  standard deviation, while categorical variables were conveyed as percentages. The Shapiro–Wilk test was used to assess normal data distribution. Differences in population homogeneity and objective image quality were both assessed using the Mann–Whitney *U* test and two-tailed *t* test for non-normal distribution and normal distribution, respectively. Linear regression analysis was performed between the best *W/L* setting and attenuation values of the abdominal aorta to obtain the O-*W/L*. Repeated measurements of variance were then used to evaluate differences in image quality and vessel sizing between the M<sub>0.6</sub>, M70, and M40+, using the B-*W/L* and O-*W/L*. Inter-observer agreement for subjective image quality scores was calculated using the Cohen kappa (*k*) statistics. These results were interpreted as follows:  $\leq 0.20$ , slight or poor agreement; 0.20–0.40, fair agreement; 0.40–0.60, moderate agreement; 0.60–0.80, good agreement;  $\geq 0.80$ , excellent agreement. All analyses were performed separately using statistical software (SPSS for Windows version 21.0, SPSS Inc., Chicago, IL, USA).

## Results

### Patient population

The study population entailed 45 patients (27 male, mean age  $65.9 \pm 10.8$  years; 18 female, mean age  $66.5 \pm 10.4$  years;  $p = 0.11$ ). Mean patient body weight and body mass index were  $74.2 \pm 17.6$  kg (male  $79.3 \pm 14.9$  kg; female  $66.6 \pm 18.9$  kg;  $p = 0.016$ ) and  $25.8 \pm 6.1$  kg/m<sup>2</sup> (male  $25.9 \pm 4.7$  kg/m<sup>2</sup>; female  $25.6 \pm 7.68$  kg/m<sup>2</sup>;  $p = 0.91$ ), respectively.

**Table 1.** Objective image quality

	M_0.6	M70	M40+	M_0.6 vs. M70	M_0.6 vs. M40+	M70 vs. M40+
HU Aorta	305.7 ± 68.8	360.7 ± 81.8	708.8 ± 168.8	< <b>0.0001</b>	< <b>0.0001</b>	< <b>0.0001</b>
Noise	13.5 ± 4.8	19.8 ± 7.0	15.2 ± 4.6	< <b>0.0001</b>	0.47	<b>0.0027</b>
CNR	21.4 ± 9.5	18.1 ± 9.3	46.2 ± 15.3	<b>0.017</b>	< <b>0.0001</b>	< <b>0.0001</b>

Significant differences are shown in bold

**Table 2.** W/L settings

	Mean Width	Mean Level	COMPARISON	Width	Level
			B-W/L M70 vs M_0.6	< <b>0.0001</b>	< <b>0.0001</b>
			O-W/L M70 vs M_0.6	< <b>0.0001</b>	< <b>0.0001</b>
			B-W/L M70 vs O-W/L M70	0.19	0.32
<b>M_0.6</b>	450	100	B-W/L M40+ vs M_0.6	< <b>0.0001</b>	< <b>0.0001</b>
<b>B-W/L M70</b>	878.6±125.7	282.5±53.8	O-W/L M40+ vs M_0.6	< <b>0.0001</b>	< <b>0.0001</b>
<b>O-W/L M70</b>	847.4±192.1	273.4±62.0	B-W/L M40+ vs O-W/L M40+	<b>0.02</b>	<b>0.03</b>
<b>B-W/L M40+</b>	1413.9±153.6	456.7±77.0	B-W/L M70 vs B-W/L M40+	< <b>0.0001</b>	< <b>0.0001</b>
<b>O-W/L M40+</b>	1350.0±320.1	428.9±96.4	O-W/L M70 vs O-W/L M40+	< <b>0.0001</b>	< <b>0.0001</b>

Significant differences are shown in bold

### Objective image evaluation

Mean attenuation in the aorta was significantly lower for M\_0.6,  $305.7 \pm 68.8$ , compared to M70,  $360.7 \pm 81.8$  ( $p = 0.008$ ), and to M40+,  $708.8 \pm 168.0$  ( $p < 0.0001$ ). Image noise was significantly lower for M40+ when compared to M70 ( $p < 0.0001$ ). No significant differences for image noise were observed between M40+ and M\_0.6 ( $p = 0.47$ ). However, the CNR of M40+ was significantly higher than M\_0.6 ( $p < 0.0001$ ). Full details are reported in Table 1.

### Window settings

A CT angiography W/L setting (width, 450 HU; level, 100 HU) was used as the reference standard for M\_0.6 [20]. The B-W/L for M70 and M40+ were chosen to represent the mean of the two observers' W and L values. For M70, the Best W was  $878.6 \pm 125.7$  and the Best L was  $282.5 \pm 53.8$ , from which we derived a rounded B-W/L of 880/280; for M40+, the Best W was  $1413.8 \pm 153.5$  and the Best L was  $456.7 \pm 77.1$ , from which we derived the rounded B-W/L of 1410/450.

A regression analysis was performed from the B-W/L and the aortic HU of both M70 and M40+. This analysis allowed us to attain the O-W/L that directly correlated with intravascular attenuation. With this information, we developed the following four equations:

$$\text{Optimized } W \text{ for } M70 = 2.3491 \times \text{HU}$$

$$\text{Optimized } L \text{ for } M70 = 0.7579 \times \text{HU}$$

$$\text{Optimized } W \text{ for } M40+ = 1.9048 \times \text{HU}$$

$$\text{Optimized } L \text{ for } M40+ = 0.6146 \times \text{HU}.$$

For M70, an Optimized W of  $847.4 \pm 192.1$  and an Optimized L of  $273.4 \pm 62.0$  were derived, resulting in an O-W/L of 850/270. For M40+, an Optimized W of  $1350.0 \pm 320.1$  and an Optimized L of  $428.9 \pm 96.4$  were calculated, resulting in an O-W/L of 1350/430. No significant differences were found between the B-W/L and the O-W/L for M70 for both W ( $p = 0.19$ ) and L ( $p = 0.32$ ) values. However, we did discover significant differences for M40+ comparisons between the B-W/L and O-W/L ( $W p = 0.02$ ,  $L p = 0.03$ ). Significant differences were also observed between M70 and M40+ for both the B-W/L ( $p < 0.0001$ ) and O-W/L ( $p < 0.0001$ ). All statistical differences are shown in Table 2.

### Subjective image evaluation

Overall image quality was significantly higher for M70 and M40+, respectively, compared to the traditional M\_0.6 when using both the Best and the Optimized W/L settings (all  $p < 0.0001$ ). No significant differences were found between M70 and M40+ for any of the categories when using the B-W/L and the O-W/L (all



**Table 3.** Subjective image quality

Values	Inter-observer ( <i>k</i> )										
	B- <i>W/L</i> M70	O- <i>W/L</i> M70	B- <i>W/L</i> M40+	O- <i>W/L</i> M40+	M_0.6	B- <i>W/L</i> M70 vs. B- <i>W/L</i> M40+	O- <i>W/L</i> M70 vs. O- <i>W/L</i> M40+	M_0.6 vs. M_0.6	B- <i>W/L</i> M70 vs. B- <i>W/L</i> M40+	O- <i>W/L</i> M70 vs. O- <i>W/L</i> M40+	M_0.6 vs. M_0.6
Sharpness	4.27 ± 0.50	4.33 ± 0.48	4.30 ± 0.46	4.31 ± 0.46	3.50 ± 0.54	0.69	0.71	0.69	0.75	0.71	0.73
Noise	4.51 ± 0.55	4.36 ± 0.61	4.43 ± 0.53	4.53 ± 0.56	2.93 ± 0.81	0.71	0.69	0.71	0.66	0.77	0.66
Calcification	4.65 ± 0.48	4.75 ± 0.44	4.70 ± 0.42	4.71 ± 0.48	3.54 ± 0.80	0.76	0.78	0.76	0.65	0.70	0.67
Overall	4.47 ± 0.35	4.47 ± 0.36	4.47 ± 0.33	4.51 ± 0.34	3.33 ± 0.48	0.75	0.72	0.75	0.69	0.68	0.66
Comparison	B- <i>W/L</i> M70 vs. M_0.6	O- <i>W/L</i> M70 vs. M_0.6	B- <i>W/L</i> M40+ vs. M_0.6	O- <i>W/L</i> M40+ vs. M_0.6	B- <i>W/L</i> M70 vs. O- <i>W/L</i> M70	B- <i>W/L</i> M40+ vs. O- <i>W/L</i> M40+	O- <i>W/L</i> M70 vs. O- <i>W/L</i> M40+	B- <i>W/L</i> M70 vs. B- <i>W/L</i> M40+	O- <i>W/L</i> M70 vs. O- <i>W/L</i> M40+	B- <i>W/L</i> M70 vs. B- <i>W/L</i> M40+	O- <i>W/L</i> M70 vs. O- <i>W/L</i> M40+
Sharpness	<0.001	<0.001	<0.001	<0.001	0.51	<0.001	<0.001	0.90	<0.001	0.79	0.65
Noise	<0.001	<0.001	<0.001	<0.001	0.20	<0.001	<0.001	0.38	<0.001	0.69	0.12
Calcification	<0.001	<0.001	<0.001	<0.001	0.33	<0.001	<0.001	0.90	<0.001	0.65	0.72
Overall	<0.001	<0.001	<0.001	<0.001	0.93	<0.001	<0.001	0.54	<0.001	0.94	0.66

Significant differences are shown in bold

$p \geq 0.12$ ). The highest value for overall image quality was reached using the Optimized *W/L* setting for M40+ ( $4.51 \pm 0.34$ ). However, the best discrimination of vascular calcifications from contrast media attenuation was reached with the O-*W/L* for M70, despite no significant differences were found when compared to the O-*W/L* for M40+ ( $p = 0.72$ ). Inter-observer agreement was good among all evaluations (all  $k \geq 0.65$ , range 0.65–0.78). Full details are available in Table 3.

No significant differences for M70 in vessel sizing were found between the B-*W/L* and O-*W/L* when compared to the traditional M\_0.6 (all  $p \geq 0.39$ ). Notably, significant overestimation was observed for M40+ using the B-*W/L* compared to M\_0.6 for both iliac and femoral arteries (all  $p \leq 0.04$ ). No significant differences were detected for any of the vessels compared to M\_0.6 when using the O-*W/L* setting for M40+ (all  $p \geq 0.16$ ). Again, no significant differences for M70 were observed for any of the vessel diameters when comparing the B-*W/L* and O-*W/L* (all  $p \geq 0.16$ ), while significant overestimation of both iliac and femoral arteries diameter was noted when applying the B-*W/L* instead of O-*W/L* for M40+ (all  $p \leq 0.03$ ). All data are shown in Table 4.

## Discussion

The purpose of this study was to determine an optimal window setting for displaying virtual monoenergetic images in order to achieve similar image impressions as the standard settings of single-energy polychromatic CT angiography. This was achieved using both a traditional and an advanced algorithm [10]. Our results show that M70 and M40+ require appropriate *W/L* settings, differing from standard settings used in CT angiography. As previously noted, both M70 and M40+ require higher *W* and *L* values compared to M\_0.6, which directly corresponds with a tendency toward higher attenuation obtained from lower virtual monoenergetic keV levels close to the k-edge of iodine (33 keV) [21]. Our results suggest that a *W/L* setting of 850/270 for M70 and 1350/430 for M40+ should be selected for optimal contrast and vessel visualization.

Appropriate window setting selection can be influenced by both observer experience and personal preferences. Therefore, we deduced a mathematical way to help standardize our results [22]. Because intravascular attenuation influences the selection of *W/L* settings, we created a regression equation to obtain the optimal correlation between *W/L* parameters (width and level) and the attenuation of the aorta [16], resulting in the O-*W/L*. Although no significant differences were found between the B-*W/L* and O-*W/L* for the M70 series, significant differences were observed between the B-*W/L* and O-*W/L* for M40+ (Fig. 1, 2, 3). Furthermore, our results also required a change in the *W/L* between M70 and M40+ for both the Best and Optimized *W/L*

**Table 4.** Vessel diameter

	B-W/L M70	O-W/L M70	B-W/L M40+	O-W/L M40+	M_0.6	COMPARISON	B-W/L M70 vs M_0.6	O-W/L M70 vs M_0.6	B-W/L M70 vs O-W/L M70	B-W/L M40+ vs M_0.6	O-W/L M40+ vs M_0.6	B-W/L M40+ Vs O-W/L M40+
<b>Aorta</b>	1.96±0.39	1.95±0.40	1.99±0.39	1.98±0.40	2.00±0.41		0.56	0.54	0.85	0.89	0.81	0.51
<b>R Iliac A.</b>	1.07±0.19	1.08±0.18	1.10±0.20	1.02±0.18	1.05±0.18		0.54	0.39	0.20	<b>0.033</b>	0.21	<b>0.0003</b>
<b>L Iliac A.</b>	1.04±0.19	1.05±0.18	1.08±0.19	1.01±0.17	1.04±0.17		0.90	0.75	0.29	<b>0.017</b>	0.16	<b>0.0003</b>
<b>R Femoral A.</b>	0.77±0.15	0.78±0.15	0.83±0.16	0.78±0.12	0.77±0.14		0.95	0.94	0.97	<b>0.003</b>	0.57	<b>0.0016</b>
<b>L Femoral A.</b>	0.75±0.15	0.76±0.16	0.81±0.14	0.78±0.14	0.78±0.14		0.47	0.66	0.16	<b>0.04</b>	0.64	<b>0.03</b>

Significant differences are shown in bold

*L* settings. This change was mainly due to the higher aortic attenuation obtained in the M40 series (708.8 HU) compared with the aortic attenuation reached with M70 (360.7 HU). These results are in accordance with the observation that lowering the keV in virtual monoenergetic images as well as the kVp in single-energy acquisitions leads to a significant increase in contrast attenuation [14], which requires an adaptation of the window settings, as Saba et al. has previously described for the evaluation of calcified carotid plaques [16].

Our findings agree with the work of Bae et al. who reported a window *W* slightly less than two times the pulmonary artery attenuation and a window *L* of half the pulmonary artery attenuation [23]. Using the O-*W*/

*L* setting, we found *W* and *L* values nearly two times greater and two-thirds less than aortic attenuation, respectively, for both M70 and M40+.

Traditional and advanced virtual monoenergetic images provided higher image quality compared to the standard M\_0.6 for each of the categories analyzed. In our study, the *W*/*L* settings did not influence subjective image quality results, likely because the B-*W*/*L* was derived from an average of two expert radiologists, while the Optimized setting showed better correlation with intravascular attenuation. In addition, the inter-observer agreement was acceptable for every category involved in this study. Therefore, virtual monoenergetic algorithms are able to provide better image quality when used with mandatory, dedicated *W*/*L* settings [9].

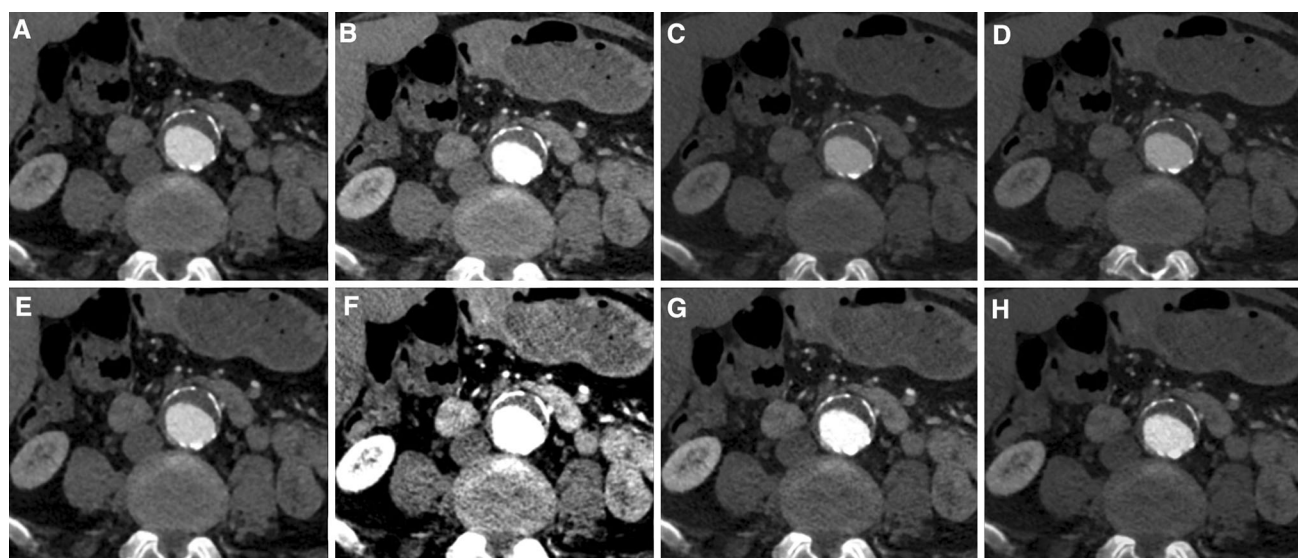


**Fig. 1.** Axial view of a CT angiography study of the abdominal aorta comparing standard M\_0.6 (A, E) to the traditional virtual monoenergetic algorithm M70 (B, C, D) and to the advanced virtual monoenergetic algorithm M40+ (F, G, H) using different *W*/*L* settings. The application of standard

M\_0.6 *W*/*L* settings to M70 (B) and to M40+ (F) reveals inadequate contrast visualization. B-*W*/*L* (C) and O-*W*/*L* (D) for M70 show comparable results. O-*W*/*L* for M40+ (H) shows better characterization of the thrombus and vascular calcifications compared to the B-*W*/*L* (G).

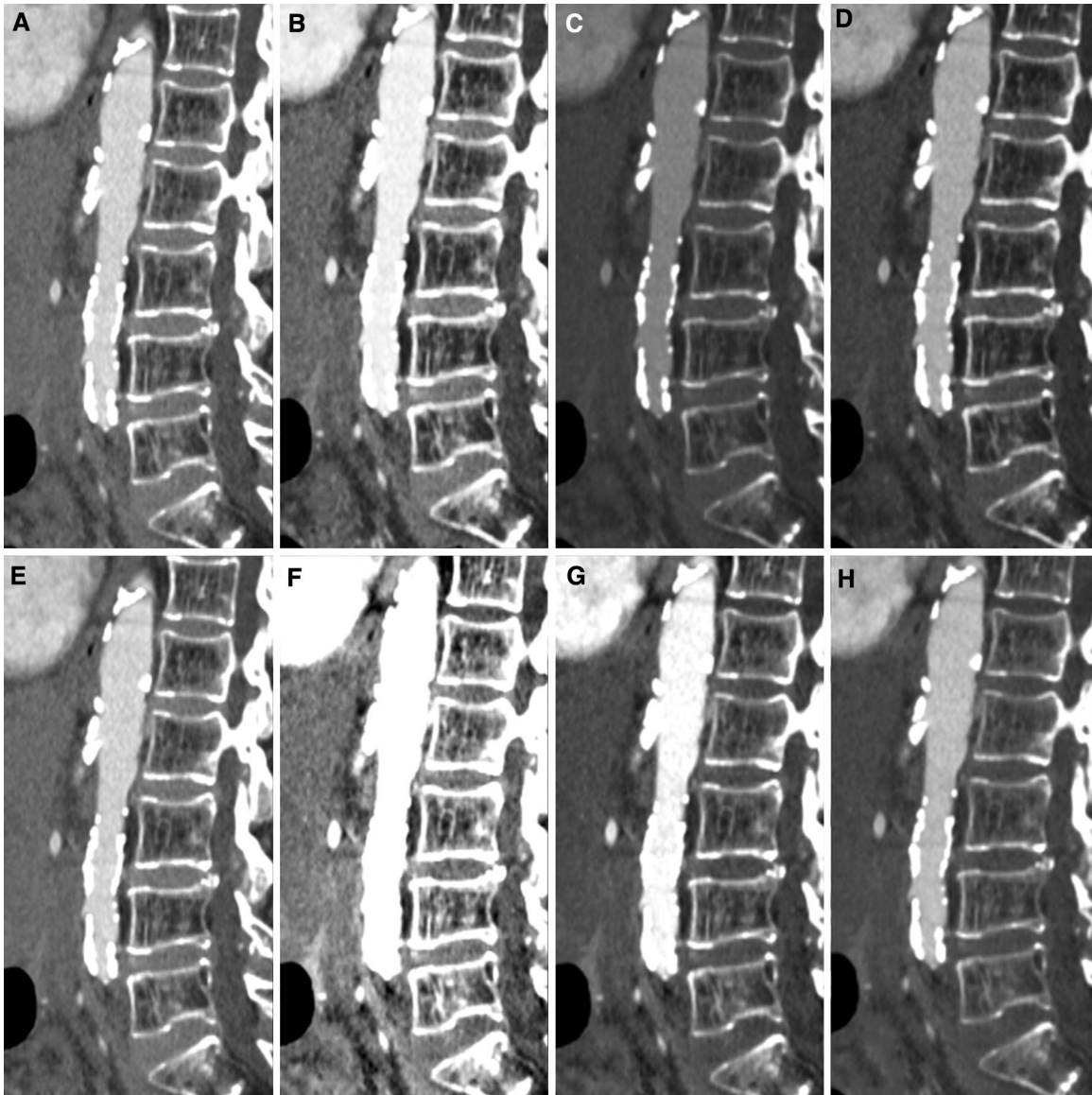


Fig. 2. Sagittal multiplanar reformation of a CT angiography study of the abdominal aorta comparing standard M<sub>0.6</sub> (A, E) to the traditional virtual monoenergetic algorithm M70 (B, C, D) and to the advanced virtual monoenergetic algorithm M40+ (F, G, H) applying different  $W/L$  settings. By using the standard M<sub>0.6</sub>  $W/L$  setting in the M70 (B) and in the M40+

(F), inadequate visualization of calcifications is noticed. For M70, B- $W/L$  (C) and O- $W/L$  (D) show comparable results. O- $W/L$  for M40+ (H) shows better characterization of vascular calcifications, in particular at the level of the superior mesenteric artery, compared to the B- $W/L$  (G).

Vessel perception may be highly influenced by selecting an incorrect  $W/L$  setting [24]. Typically, each radiologist manually adjusts  $W/L$  settings until their own optimal visualization is reached, but this did not provide enough accuracy, as reported in Table 4. For small vessels, such as common iliac and femoral arteries, we observed systematic overestimation of vessel diameters. This was highlighted using the B- $W/L$  for M40+ compared to the standard M<sub>0.6</sub>. These differences were corrected through the use of a dedicated and O- $W/L$  that compensated for vasculature blurring and reduced inter-measurement variability, probably due to the use of a

narrower  $W$  value [24] compared with the B- $W/L$ ; these results were also confirmed by the M70 analysis, where a narrow  $W$  value was applied and no overestimation was observed.

Our regression analysis showed that the selection of O- $W/L$  settings based on intravascular attenuation is advisable. However, multiplying  $W$  and  $L$  values for intravascular attenuation [16, 23] is time intensive, which may be a limitation for clinical implementation. Therefore, considering the increasing implementation of single-energy low kVp acquisition protocols and the growing availability of DECT with low keV virtual imaging

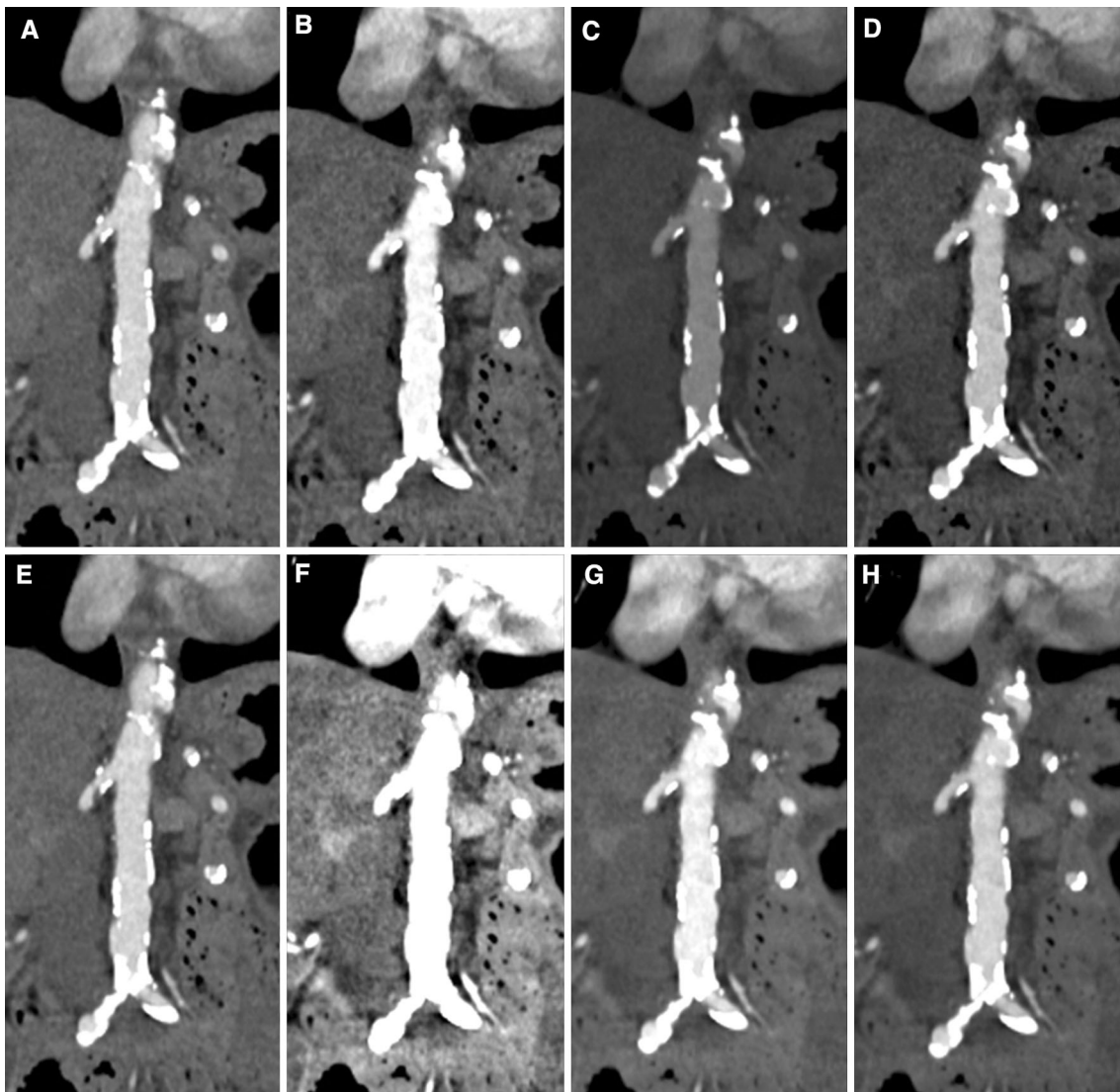


**Fig. 3.** Coronal multiplanar reformation of a CT angiography study of the abdominal aorta comparing standard M<sub>0.6</sub> (A, E) to the traditional virtual monoenergetic algorithm M70 (B, C, D) and to the advanced virtual monoenergetic algorithm M40+ (F, G, H) using different *W/L* settings. The application of standard M<sub>0.6</sub> *W/L* settings to M70 (B) and to M40+ (F) re-

veals inadequate visualization of aortic wall calcifications. For M70, B-*W/L* (C) and O-*W/L* (D) show comparable results. For M40+, O-*W/L* (H) shows better characterization of aortic wall calcifications, in particular at the level of the aortic bifurcation, compared to the B-*W/L* (G).

capabilities, dedicated software to automate this task would be highly desirable. This software would be able to automatically select and adapt *W/L* settings to high intravascular attenuation and *ipso facto* to low keV levels.

We do acknowledge that our study has limitations. First, we did not apply the traditional *W/L* setting (450/100) for M<sub>0.6</sub> to the M70 and M40+ series in the subjective image quality analysis. This was informed by our hypothesis that the traditional *W/L* settings were not adequate for M70 and M40+ due to the significant differences in intravascular attenuation. Second, no inter-observer agreement analysis was performed on *W/*

*L* values regarding the possible single HU variation of the *W* and *L* values. Third, our results are confined to dual-source DECT users. Further studies focused on other DECT technologies (e.g., multi-layer spectral and rapid kV switching DECT) are advisable. Lastly, no diagnostic accuracy analysis was performed, as that was not the primary goal of this study.

In conclusion, our study shows that traditional and advanced virtual monoenergetic CT angiography requires O-*W/L* settings. In addition, both M70 and M40+ require different window settings. Finally, we suggest using an O-*W/L* setting of 850/270 for M70 and of 1350/430 for M40+.



### Compliance with ethical standards

**Funding** No funding was received for this study.

**Conflict of interest** Schoepf is a consultant for and/or receives research support from Astellas, Bayer, Bracco, GE, Guerbet, Medrad, and Siemens. The other authors declare that they have no conflict of interest.

**Ethical approval** All procedures performed in studies involving human participants were in accordance with the ethical standards of the institutional and/or national research committee and with the 1964 Helsinki declaration and its later amendments or comparable ethical standards. For this type of study formal consent is not required.

**Informed consent** Statement of informed consent was not applicable since the manuscript does not contain any patient data.

### References

- Krauss B, Grant KL, Schmidt BT, Flohr TG (2015) The importance of spectral separation: an assessment of dual-energy spectral separation for quantitative ability and dose efficiency. *Invest Radiol* 50(2):114–118. doi:10.1097/rli.000000000000109
- Flohr TG, Klotz E, Allmendinger T, et al. (2010) Pushing the envelope: new computed tomography techniques for cardiothoracic imaging. *J Thorac Imaging* 25(2):100–111. doi:10.1097/RTI.0b013e3181d7e898
- He J, Wang Q, Ma X, Sun Z (2015) Dual-energy CT angiography of abdomen with routine concentration contrast agent in comparison with conventional single-energy CT with high concentration contrast agent. *Eur J Radiol* 84(2):221–227. doi:10.1016/j.ejrad.2014.11.025
- Carrascosa P, Leipsic JA, Capunay C, et al. (2015) Monochromatic image reconstruction by dual energy imaging allows half iodine load computed tomography coronary angiography. *Eur J Radiol* 84(10):1915–1920. doi:10.1016/j.ejrad.2015.06.019
- Maturen KE, Kaza RK, Liu PS, et al. (2012) “Sweet spot” for endoleak detection: optimizing contrast to noise using low keV reconstructions from fast-switch kVp dual-energy CT. *J Comput Assist Tomogr* 36(1):83–87. doi:10.1097/RCT.0b013e31824258cb
- Secchi F, De Cecco CN, Spearman JV, et al. (2015) Monoenergetic extrapolation of cardiac dual energy CT for artifact reduction. *Acta radiologica* 56(4):413–418. doi:10.1177/0284185114527867
- Bamberg F, Dierks A, Nikolaou K, et al. (2011) Metal artifact reduction by dual energy computed tomography using monoenergetic extrapolation. *Eur Radiol* 21(7):1424–1429. doi:10.1007/s00330-011-2062-1
- Mangold S, Cannao PM, Schoepf UJ, et al. (2015) Impact of an advanced image-based monoenergetic reconstruction algorithm on coronary stent visualization using third generation dual-source dual-energy CT: a phantom study. *Eur Radiol*. doi:10.1007/s00330-015-3997-4
- Sudarski S, Apfaltrer P, Nance JW Jr, et al. (2013) Optimization of keV-settings in abdominal and lower extremity dual-source dual-energy CT angiography determined with virtual monoenergetic imaging. *Eur J Radiol* 82(10):e574–e581. doi:10.1016/j.ejrad.2013.04.040
- Grant KL, Flohr TG, Krauss B, et al. (2014) Assessment of an advanced image-based technique to calculate virtual monoenergetic computed tomographic images from a dual-energy examination to improve contrast-to-noise ratio in examinations using iodinated contrast media. *Invest Radiol* 49(9):586–592. doi:10.1097/RLI.000000000000060
- Wichmann JL, Gillott MR, De Cecco CN, et al. (2015) Dual-energy computed tomography angiography of the lower extremity runoff: impact of noise-optimized virtual monochromatic imaging on image quality and diagnostic accuracy. *Invest Radiol*. doi:10.1097/rli.0000000000000216
- Pinho DF, Kulkarni NM, Krishnaraj A, Kalva SP, Sahani DV (2013) Initial experience with single-source dual-energy CT abdominal angiography and comparison with single-energy CT angiography: image quality, enhancement, diagnosis and radiation dose. *Eur Radiol* 23(2):351–359. doi:10.1007/s00330-012-2624-x
- Albrecht MH, Scholtz JE, Husers K, et al. (2015) Advanced image-based virtual monoenergetic dual-energy CT angiography of the abdomen: optimization of kiloelectron volt settings to improve image contrast. *Eur Radiol*. doi:10.1007/s00330-015-3970-2
- Beeres M, Trommer J, Frellesen C, et al. (2015) Evaluation of different keV-settings in dual-energy CT angiography of the aorta using advanced image-based virtual monoenergetic imaging. *Int J Cardiovasc Imaging*. doi:10.1007/s10554-015-0728-5
- Meier A, Wurnig M, Desbiolles L, et al. (2015) Advanced virtual monoenergetic images: improving the contrast of dual-energy CT pulmonary angiography. *Clin Radiol*. doi:10.1016/j.crad.2015.06.094
- Saba L, Mallarin G (2009) Window settings for the study of calcified carotid plaques with multidetector CT angiography. *AJNR Am J Neuroradiol* 30(7):1445–1450. doi:10.3174/ajnr.A1509
- Meyer M, Haubenreisser H, Schoepf UJ, et al. (2014) Closing in on the K edge: coronary CT angiography at 100, 80, and 70 kV-initial comparison of a second-versus a third-generation dual-source CT system. *Radiology* 273(2):373–382. doi:10.1148/radiol.14140244
- Goshima S, Kanematsu M, Kondo H, et al. (2013) Preoperative planning for endovascular aortic repair of abdominal aortic aneurysms: feasibility of nonenhanced MR angiography versus contrast-enhanced CT angiography. *Radiology* 267(3):948–955. doi:10.1148/radiol.13121557
- Rubin GD, Schmidt AJ, Logan LJ, Sofilos MC (2001) Multi-detector row CT angiography of lower extremity arterial inflow and runoff: initial experience. *Radiology* 221(1):146–158. doi:10.1148/radiol.2211001325
- Schueler-Weidekamm C, Schaefer-Prokop CM, Weber M, Herold CJ, Prokop M (2006) CT angiography of pulmonary arteries to detect pulmonary embolism: improvement of vascular enhancement with low kilovoltage settings. *Radiology* 241(3):899–907. doi:10.1148/radiol.2413040128
- Riederer SJ, Mistretta CA (1977) Selective iodine imaging using K-edge energies in computerized X-ray tomography. *Med Phys* 4(6):474–481
- Zou KH, Tuncali K, Silverman SG (2003) Correlation and simple linear regression. *Radiology* 227(3):617–622. doi:10.1148/radiol.2273011499
- Bae KT, Mody GN, Balfe DM, et al. (2005) CT depiction of pulmonary emboli: display window settings. *Radiology* 236(2):677–684. doi:10.1148/radiol.2362041558
- Liu Y, Hopper KD, Mauger DT, Addis KA (2000) CT angiographic measurement of the carotid artery: optimizing visualization by manipulating window and level settings and contrast material attenuation. *Radiology* 217(2):494–500. doi:10.1148/radiology.217.2.r00oc32494